Available online at www.sciencedirect.com

ScienceDirect

Energy Procedia 63 (2014) 4224 – 4239

Energy Procedia

GHGT-12

CO_2 storage monitoring: leakage detection and measurement in subsurface volumes from 3D seismic data at Sleipner

R. Andrew Chadwick[1]*, Benjamin P. Marchant[1], Gareth A. Williams[1]

[1]*British Geological Survey, Nottingham, NG12 5GG, England, UK.*

Abstract

Demonstrating secure containment is a key plank of CO_2 storage monitoring. Here we use the time-lapse 3D seismic surveys at the Sleipner CO_2 storage site to assess their ability to provide robust and uniform three-dimensional spatial surveillance of the Storage Complex and provide a quantitative leakage detection tool. We develop a spatial-spectral methodology to determine the actual detection limits of the datasets which takes into account both the reflectivity of a thin CO_2 layer and also its lateral extent. Using a tuning relationship to convert reflectivity to layer thickness, preliminary analysis indicates that, at the top of the Utsira reservoir, CO_2 accumulations with pore volumes greater than about 3000 m^3 should be robustly detectable for layer thicknesses greater than one metre, which will generally be the case. Making the conservative assumption of full CO_2 saturation, this pore volume corresponds to a CO_2 mass detection threshold of around 2100 tonnes. Within the overburden, at shallower depths, CO_2 becomes progressively more reflective, less dense, and correspondingly more detectable, as it passes from the dense phase into a gaseous state. Our preliminary analysis indicates that the detection threshold falls to around 950 tonnes of CO_2 at 590 m depth, and to around 315 tonnes at 490 m depth, where repeatability noise levels are particularly low. Detection capability can be equated to the maximum allowable leakage rate consistent with a storage site meeting its greenhouse gas emissions mitigation objective. A number of studies have suggested that leakage rates around 0.01% per year or less would ensure effective mitigation performance. So for a hypothetical large-scale storage project, the detection capability of the Sleipner seismics would far exceed that required to demonstrate the effective mitigation leakage limit. More generally it is likely that well-designed 3D seismic monitoring systems will have robust 3D detection capability significantly superior to what is required to prove greenhouse gas mitigation efficacy.

Peer-review under responsibility of the Organizing Committee of GHGT-12

Keywords: CO2 storage, monitoring, Sleipner, leakage, detection, 3D seismic, time-lapse sesimic

* Corresponding author. Tel.: +44-115-9363183
E-mail address: rach@bgs.ac.uk

Peer-review under responsibility of the Organizing Committee of GHGT-12
doi:10.1016/j.egypro.2014.11.458

1. Introduction

Under the European CO_2 Storage Directive [1], the operator needs to demonstrate 'zero detectable leakage' in order to close a storage site and transfer responsibility to the national authority. In this context, leakage is defined as the subsurface escape of CO_2 from the defined Storage Complex, the top of which would normally lie at some level within the overburden. Time-lapse 3D seismic surveys are unique in their ability to provide robust and uniform three-dimensional spatial surveillance of the Storage Complex and provide a very powerful leakage monitoring tool because of their ability to detect small changes in fluid content of the overburden rock volume above the storage reservoir. Here we analyse statistically the ability of 3D time-lapse seismic to detect small amounts of CO_2 migration in the overburden above the storage reservoir.

The Sleipner CO_2 storage operation in the Norwegian sector of the Central North Sea [2, 3] commenced in 1996 and currently stores around 15 million tonnes of CO_2 in the Utsira Sand, a giant saline aquifer. It has a comprehensive time-lapse 3D seismic monitoring programme with a baseline survey acquired in 1994 and a number of repeat surveys in the years following [4]. The seismic data image the CO_2 in the reservoir as a brightly reflective multi-layer plume [5]. Here we focus on the capability of the time-lapse seismic data to detect small changes in the overburden and thereby to establish quantitative detection thresholds on migrating CO_2 in the overburden.

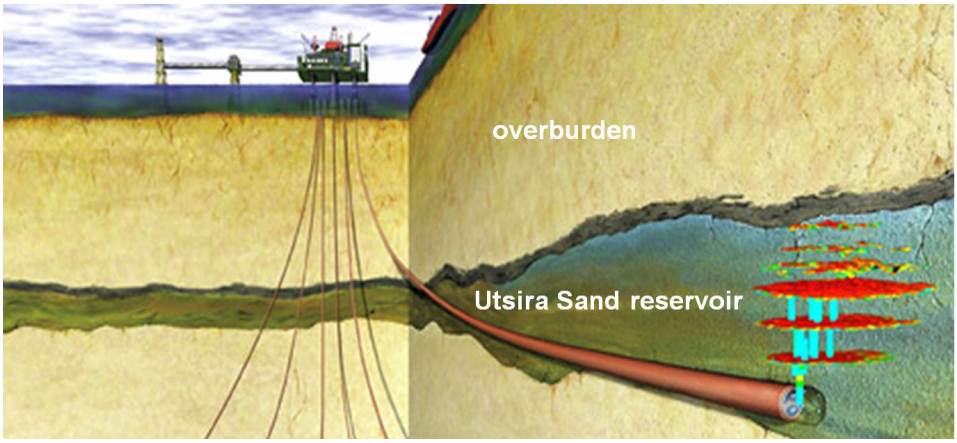

Fig. 1. Schematic diagram of the Sleipner injection operation, showing the storage reservoir, the layered CO_2 plume and the overburden (image courtesy of Statoil ASA)

2. Seismic signatures of small CO_2 accumulations

Accumulations of CO_2 in the overburden are likely to occur within higher permeability regions, either as sub-vertical columns ('chimneys') of vertically migrating CO_2, or as thin sub-horizontal layers of ponded CO_2 which grow laterally. In both cases 'difference' signal will be produced on time-lapse seismics, either via a reflection from the accumulation itself, or by velocity-pushdown inducing measurable time-shifts in the underlying reflector sequence that produce a difference response (Fig. 2).

It has been shown [6] that statistical analysis of very small time-shifts on 3D seismics can constrain CO_2 amounts in the overburden. Here we take a different approach and focus on induced reflectivity changes due to small CO_2 accumulations. The analysis involves the detection of small reflectivity changes attributable to CO_2 within a 3D cloud of repeatability noise which is not related to the presence of CO_2. This section introduces a novel statistical

methodology to determine the detectability of small reflectivity changes based upon their brightness and spatial extent.

The methodology is in two stages:

- Selection of a reproducible method to identify reflection signal within a noisy dataset
- Simulation tests to explore the probability of detecting signals of variable spatial extent and reflection amplitude.

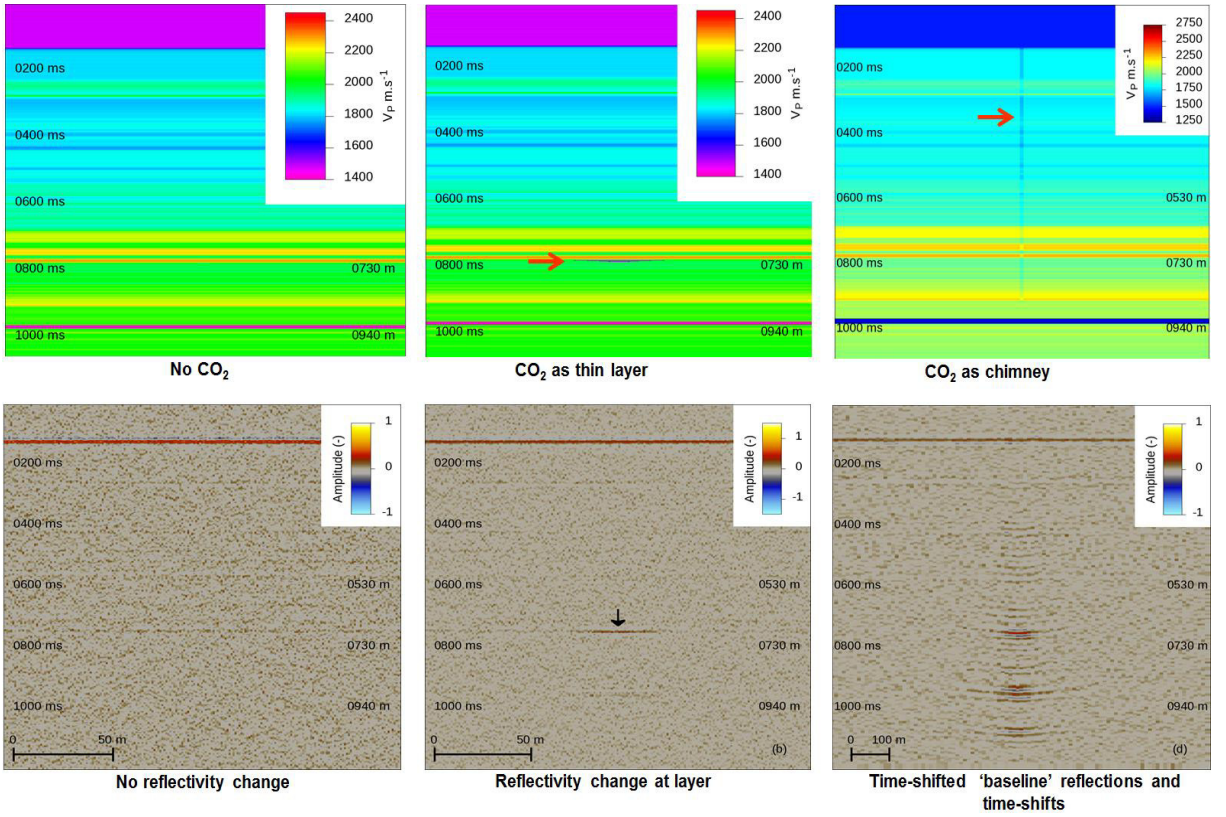

Fig. 2. Simplified Sleipner velocity models (top) with the reservoir top at about 900 ms (two-way time). Models have no CO_2 (left), a thin wedge of CO_2 (middle) and a vertical CO_2 chimney (right). Synthetic difference seismic profiles (bottom) show difference noise (left) and changes induced by the CO_2 either as a reflection (middle) or as a time-shift difference response (right).

2.1. Sleipner time-lapse data

The time-lapse seismic datasets from Sleipner (Fig. 3) show differences in seismic response between the 1994 (baseline) survey and the first repeat survey in 1999, with the CO_2 plume imaged as a brightly reflective tiered feature in the Utsira Sand. Of particular note is the observation that the injected CO_2 had reached the topseal of the Utsira reservoir just prior to the 1999 survey, with accumulations of CO_2 visible on the difference data as two small bright reflections (Fig. 3). Difference signal in the overburden is not due to CO_2, but rather is composed of random noise components plus systematic repeatability noise where the geology and naturally-occurring gas pockets are

strongly reflective. Parts of the overburden are 'quiet' and would have a high detection capability, whereas other parts are noisier with poorer detection capability.

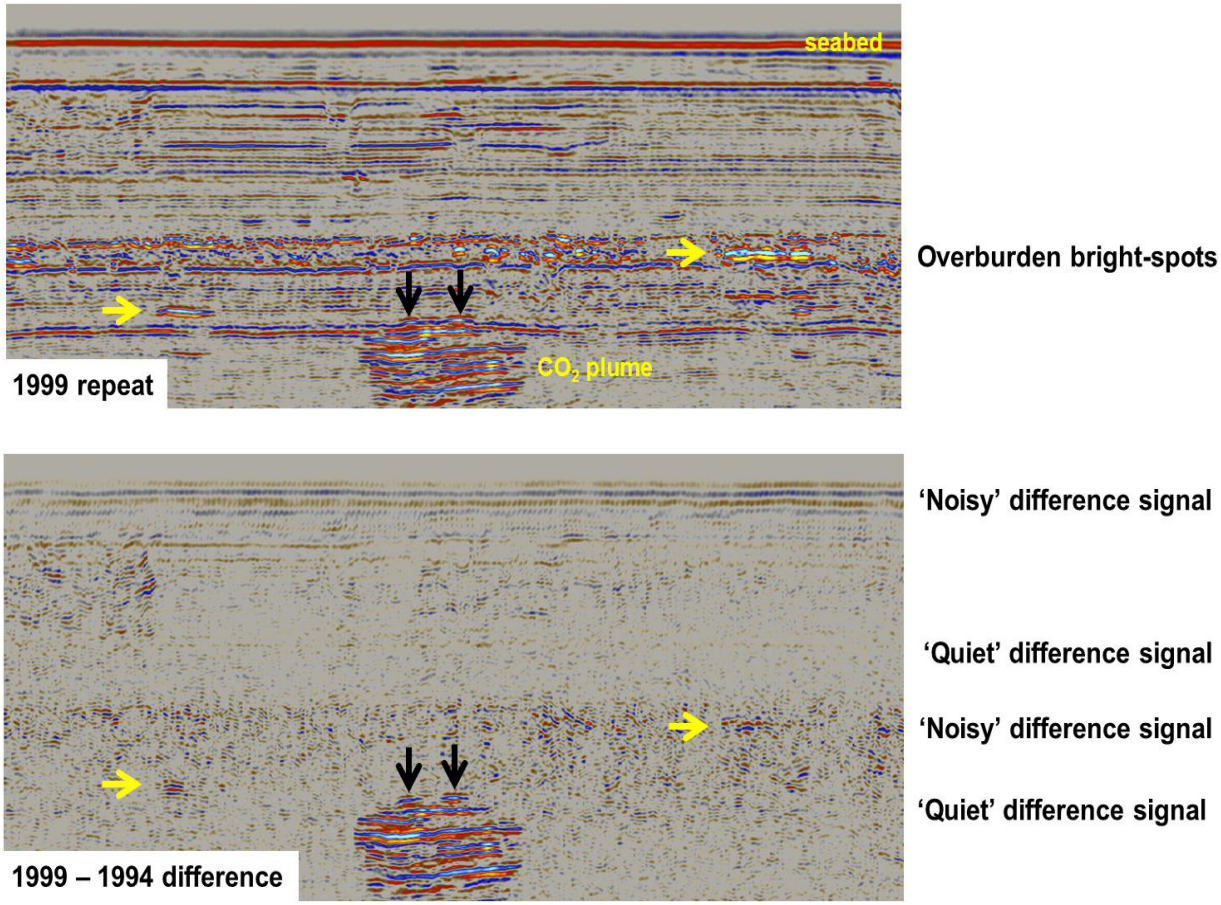

Fig. 3. Seismic inline through the reflective CO_2 plume and overburden showing the 1999 repeat survey (top) and the 1999-1994 difference data (bottom). Note prominent bright-spots in the overburden due to natural gas (yellow arrows) and at the top of the reservoir due to CO_2 (black arrows). Seismic sections show two-way time range of 0-1200 ms.

The two small lenses of CO_2 accumulating beneath the reservoir topseal in 1999 (Fig. 3) can be mapped on the difference data (Fig. 4). They clearly show reflection amplitude characteristics distinct from the rest of the top reservoir surface, being brighter and of greater lateral extent (Fig. 4b). From the reflection amplitudes [7], the pore volumes of the two accumulations can be estimated at about 9000 and 11000 m^3 respectively. Other features on the difference map can be attributed to the repeatability noise effects noted above, arising from small intrinsic mismatches between the 1994 (baseline) and 1999 surveys. It is clear that the level of repeatability noise plays a key role in determining the detectability threshold. So, for a patch of CO_2 to be identified correctly, it must be robustly distinguishable from the largest noise peaks. This will depend both on its brightness (reflection amplitudes) and also on its spatial extent.

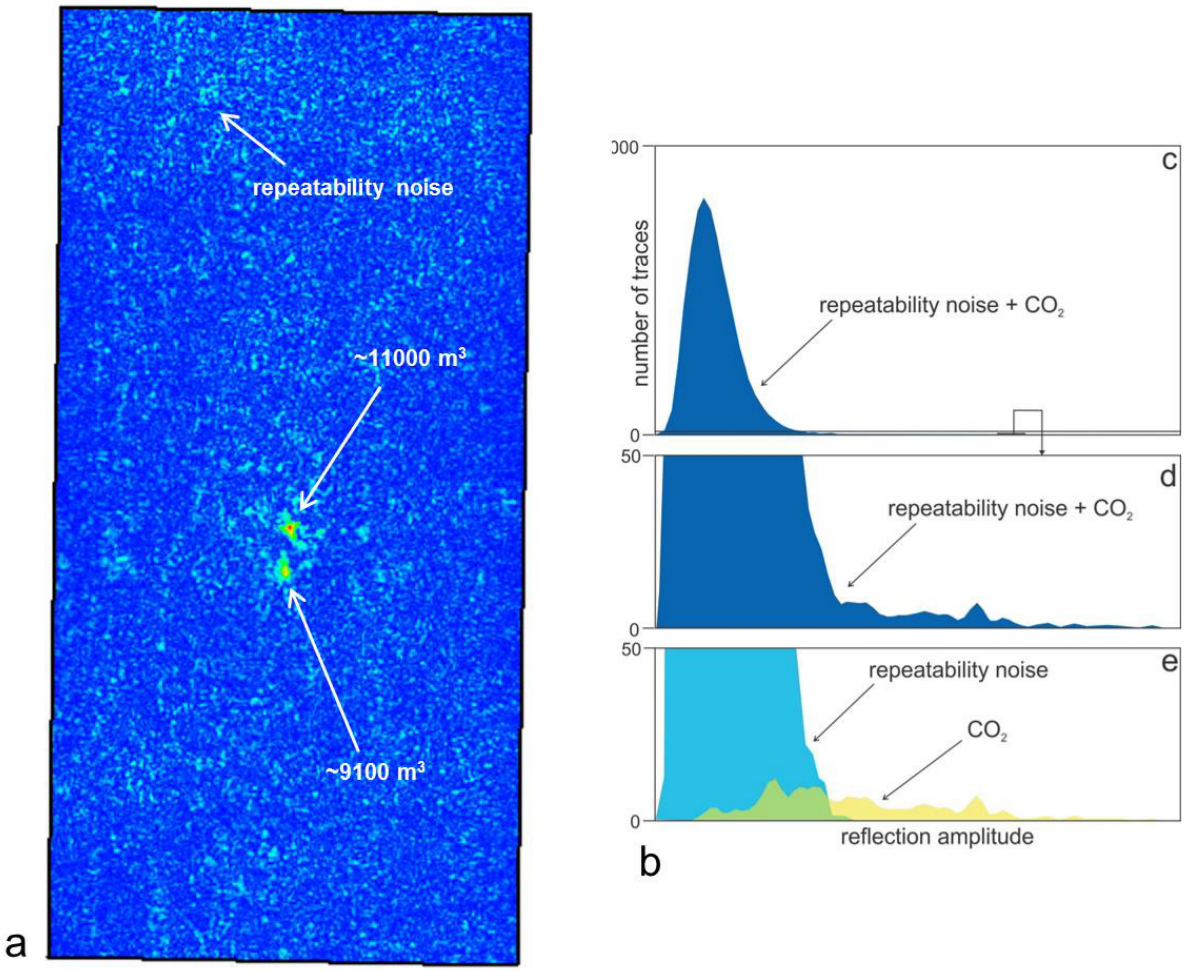

Fig. 4. a) Map of reflection amplitude differences at top Utsira Sand (displaying top Utsira horizon slice), showing two small accumulations of CO_2 at the reservoir top (b) histogram showing amplitude distributions on the top Utsira horizon slice

3. Detecting plumes within noisy images by statistical analysis of spatial and amplitude components

A discrete wavelet transform (DWT) is used to discriminate between the plume and the noise within the image [8, 9]. The DWT decomposes the image into components that each correspond to variation over a different spatial scale. Each component can then be de-noised or filtered separately. This makes it possible to efficiently remove complex and spatially correlated noise components.

To illustrate the principle, we initially use the DWT on a 1-D data example, comprising a north-south cross-section through the two CO_2 accumulations (Fig. 5). The nature of the difference signal in terms of real CO_2

accumulations contrasted with repeatability noise is clear; the CO_2 signal is of significantly higher amplitude, and generally of greater coherent spatial extent, than the surrounding noise (Fig. 5b).

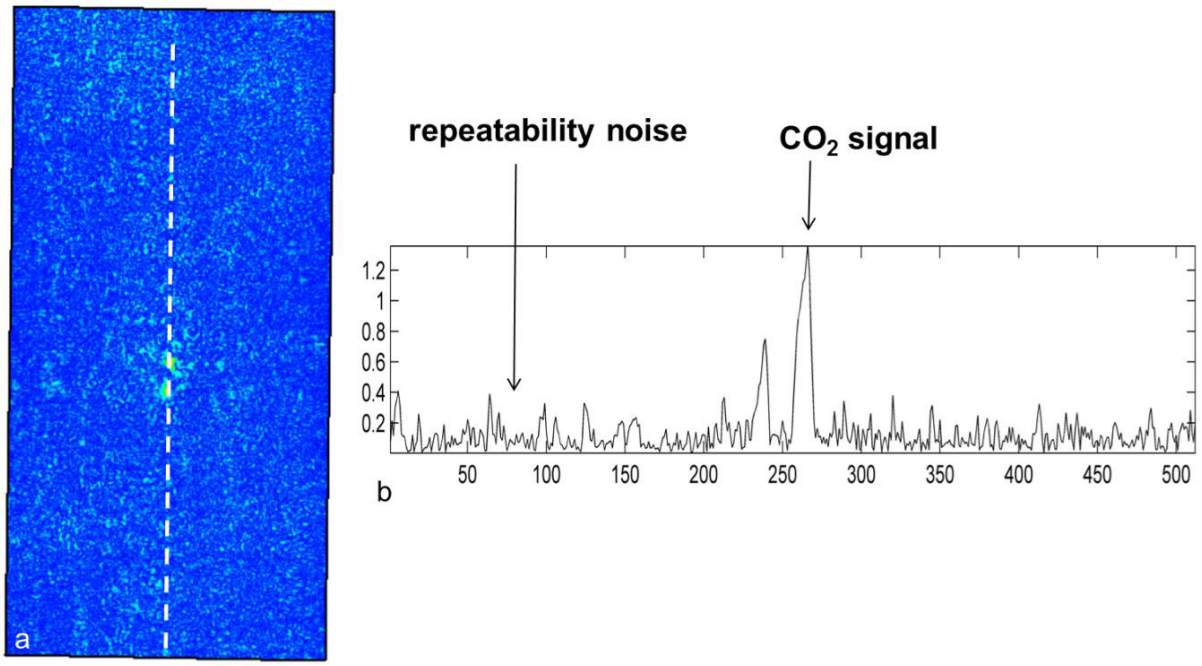

Fig. 5. a) Map of reflection amplitude differences at top Utsira Sand, showing line of section in b) as white dashed line. b) South-north section through two small accumulations at the reservoir top showing amplitude variations.

The 1-D wavelet de-noising procedure is illustrated in Fig. 6. The observed signal is shown in the top left graph. The red plots below this are the different components of the DWT of this signal, using a spatial decomposition based on the simple Haar wavelet [10]. The first component corresponds to variation over a nominal spatial scale of 2 to 4 trace spacings (25 to 50 m). The second corresponds to a scale of 4 to 8 trace spacings (50 to 100m), the third to scale of 8 to 16 (100 to 200m) and the fourth to a scale of 16 to 32 (200 to 400m). The remaining variation over longer scales is contained in the fifth 'approximation' component. If these five components are summed then the original signal is reformed.

The DWT expresses each spatial component by a set of location-specific coefficients (Fig. 6b), the number of coefficients decreasing as the length of the scale increases. From the coefficients it is possible to calculate each of the scale components (Fig. 6a) and by summing these components the signal can be reproduced (Fig. 6a, top). We refer to this process as signal reconstruction.

The wavelet de-noising method aims to set those co-efficients caused purely by noise to zero, thereby removing noise from the reconstructed signal. Generally a threshold (T) is selected for each spatial component and can vary between components. Coefficients with absolute values less than this threshold are set to zero. In hard-thresholding the remaining coefficients are unaltered. In soft-thresholding the absolute values of the remaining parameters are reduced by T. Soft-thresholding prevents unrealistic sharp discontinuities appearing in the de-noised signal. However it also has the effect of reducing the magnitude of the features of interest.

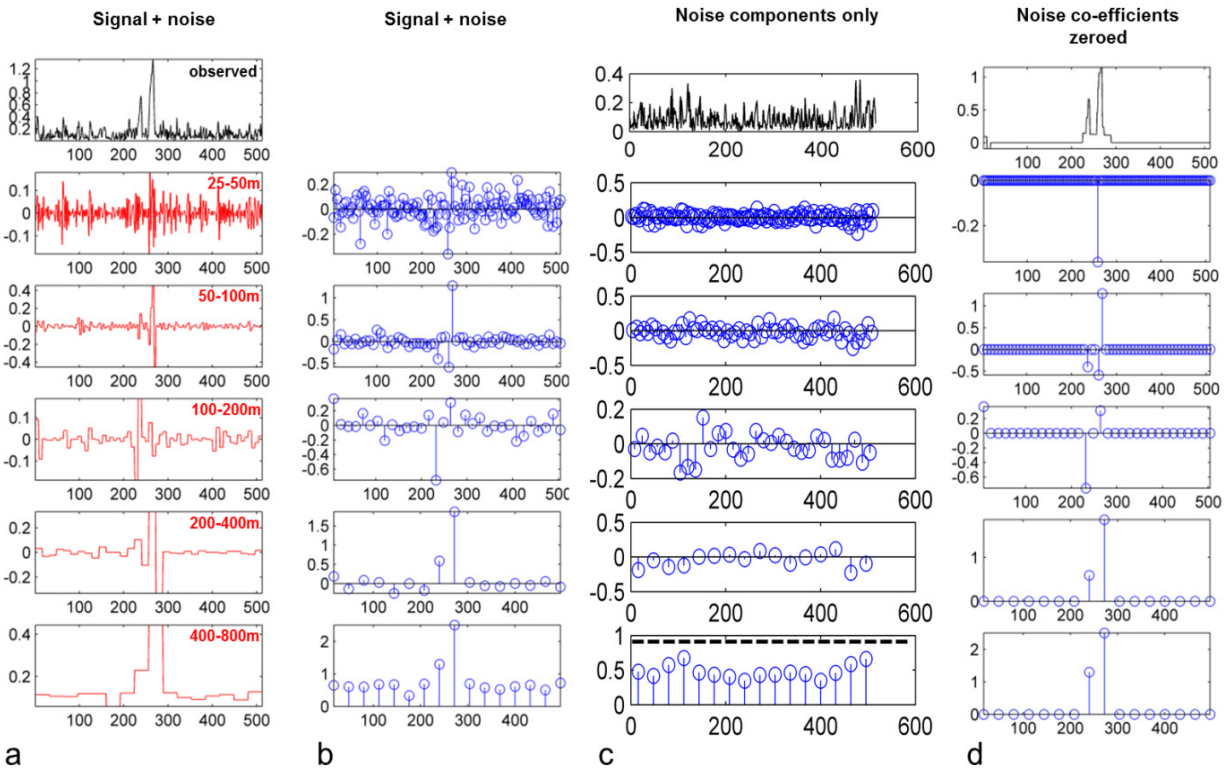

Fig. 6. Wavelet de-noising of the 1-D signal in Fig. 5. a) Observed signal prior to de-noising (top) and scale components of signal determined from the DWT (lower), b) DWT co-efficients for each scale, c) Observed signal from a different cross-section containing only noise (top) and scale components including a schematic thresholding level (dashed line), d) De-noised signal (top), thresholded DWT parameters (lower).

If the noise is known to be random and Gaussian then the optimal thresholding values can be determined from the variance of the noise. However the noise in the Sleipner image has some spatial correlation or structure, so we adapt our threshold values such that they are suited to our particular image. We do this by calculating the DWT of a signal from a cross-section which is known to contain only noise (Fig. 6c) and determine the magnitude of coefficients that arise for each scale. In this illustrative example we set our threshold coefficient for each scale at 1.5 times the maximum coefficient observed for that scale in the DWT of the noise. More sophisticated methods for selecting the threshold may be deployed as appropriate.

The DWT parameters after hard thresholding are illustrated (Fig. 6d) together with the de-noised signal reconstructed from the coefficients (Fig. 6d, top). The noise has been removed from this signal although there is an artefact on the far-left of the signal and possibly a second artefact between the two peaks of the plume.

3.1. De-noising 2-D images (maps)

Applying a similar de-noising procedure to the mapped image of reflectivity change (Fig. 5a), two 128 × 256 trace portions of the image were extracted such that the CO_2 accumulations are fully contained within one of the extracted areas, with the other one containing only noise (Fig. 7).

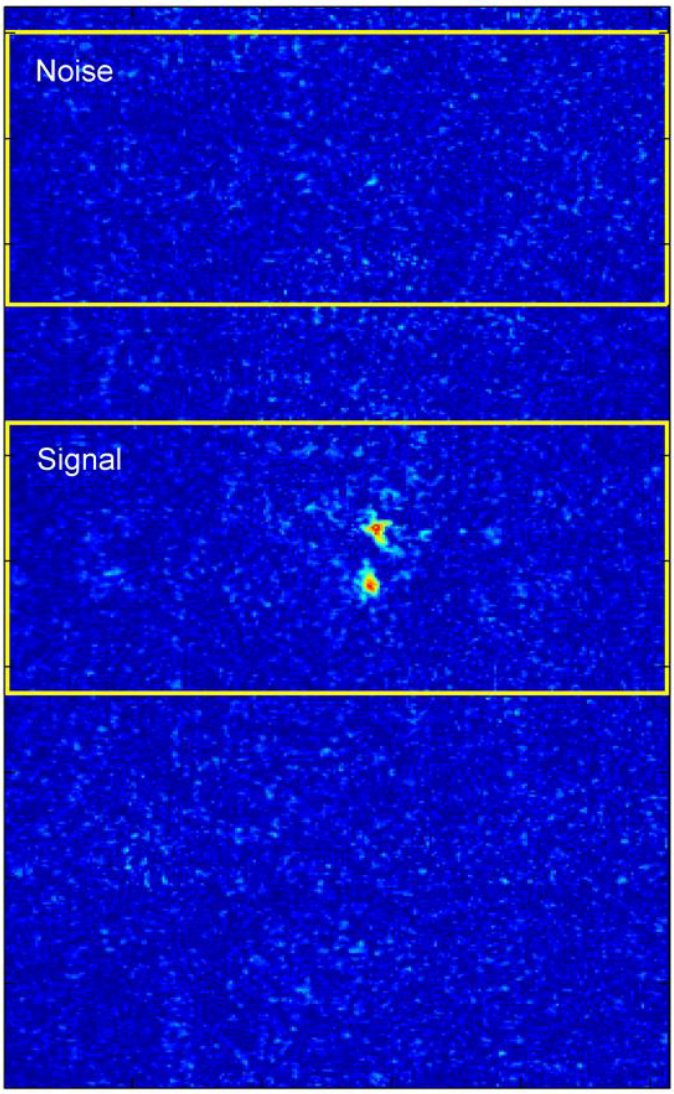

Fig. 7. Map of reflection amplitude differences at top Utsira Sand, showing one of the rectangular extracted areas containing purely noise and the other containing CO_2 signal + noise

Applying the DWT (Fig. 8) shows the different spatial components that result for these images, and histograms of the DWT coefficients for each component. The de-noising threshold for each component was again set to 1.5 times the largest DWT coefficient for that spatial component in the noise portion of the image and both hard and soft thresholding was applied to the image containing the CO_2 signal.

De-noised images from the two thresholding methods are shown (Fig. 9a) together with a cross-section through the area (Fig. 9b). Two small separate areas of CO_2 signal are extracted. The reduction in reflection amplitude (brightness) caused by soft thresholding is clearly evident. On the other hand, hard thresholding leads to a number of small extracted artefacts amongst the noise portion of the image.

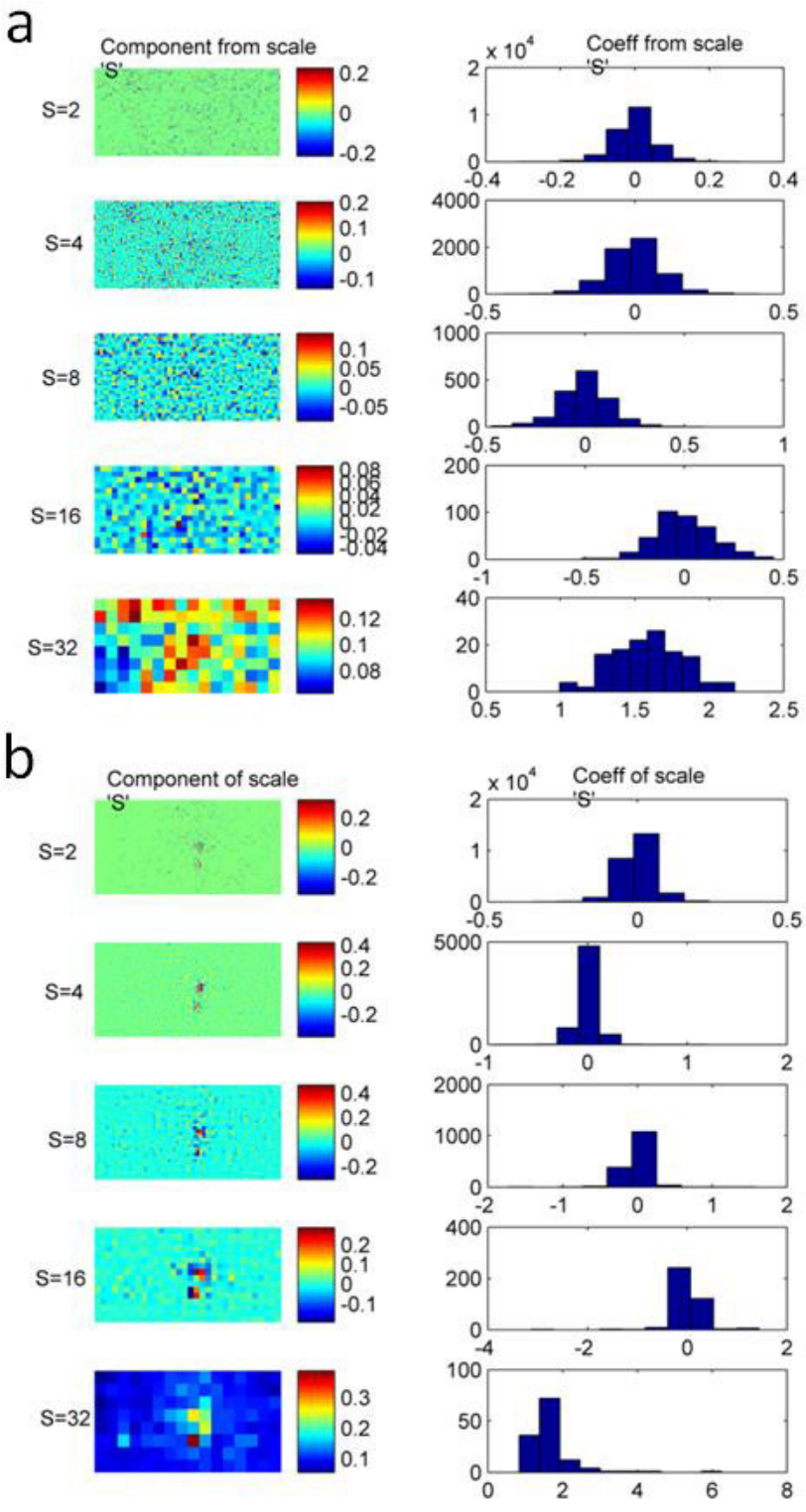

Fig. 8. a) DWT of noise-only area extract b) DWT of CO_2 signal plus noise area extract

The pros and cons of each thresholding method need assessing from more datasets, but for the remainder of this study we implement a 'hybrid' combination of the two methods. Using soft thresholding we identify the spatial extent of the CO_2 signal, and all traces with amplitude greater than 0.05 are assumed to be part of the CO_2 signal. Within this group of traces amplitudes are then assigned from the hard thresholded image (Fig. 9a).

The notional 'volume' of the 'hybrid' extracted seismic traces (number of traces × average amplitude of these traces) is equal to 164.7. This can be converted to true pore volume by scaling reflection amplitude to thickness [7], multiplying by the trace area (equal to the seismic bin area) and assuming an average porosity. Using a trace area of 156.25 m^2 (12.5 m x 12.5 m) and assuming a porosity of 0.37 gives a combined pore volume for the extracted traces of 20844 m3. This compares closely with a combined pore volume of 20157 m^3 for the two CO_2 accumulations as manually interpreted on the data.

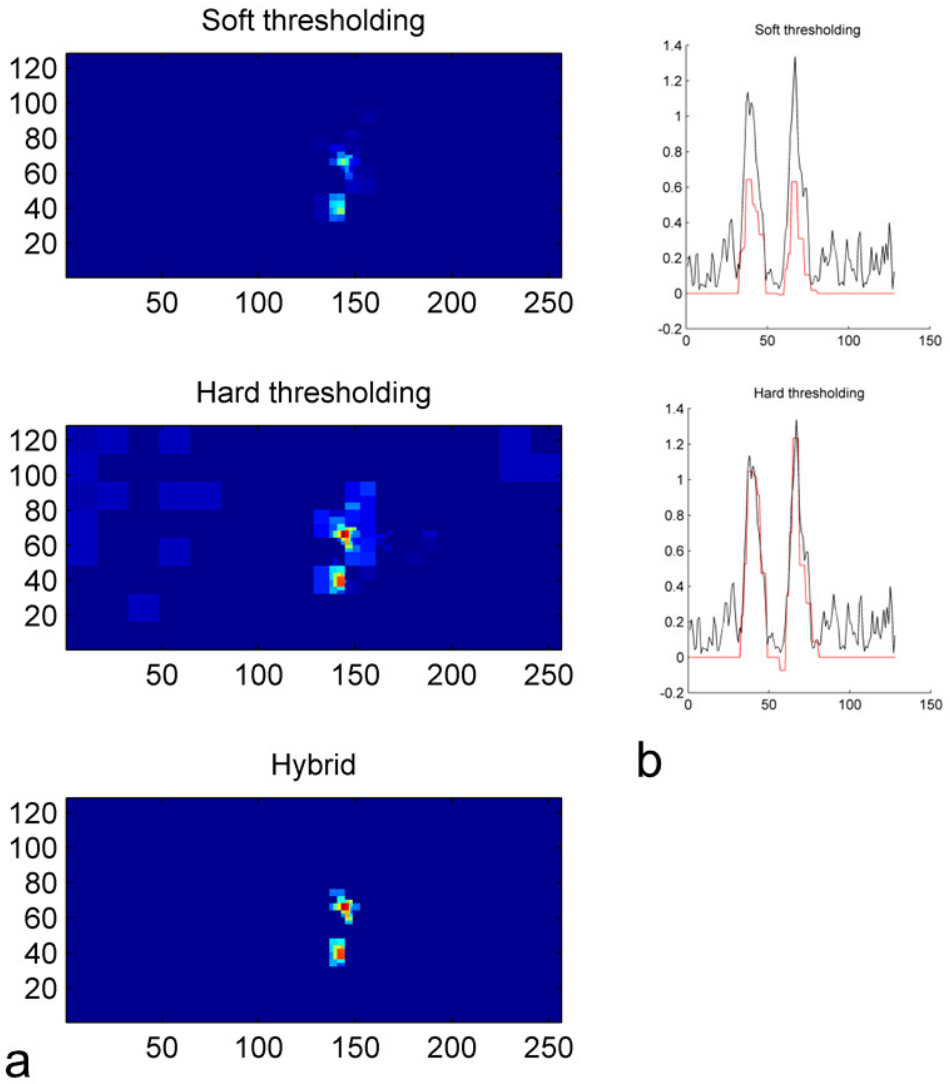

Fig. 9. Extracted CO_2 signals after thresholding b) cross-section through CO_2 signals image after soft and hard thresholding (black line shows original data, red line shows extracted de-noised signal)

3.2. Uncertainty

The pore volume estimate relies upon a statistical model and de-noising algorithm and so is subject to uncertainty. A different volume estimate could result if the plume were positioned differently with respect to the background noise. This uncertainty was quantified by repeatedly superimposing the extracted CO_2 signal upon variably noisy portions of the seismic map. For a thousand iterations the position of the extracted CO_2 signal was randomly selected and the wavelet de-noising procedure was applied. The histogram of errors, the difference between the volume of the superimposed CO_2 signal and the newly extracted CO_2 signal, allows confidence limits for the estimated pore volume to be determined (Fig. 10).

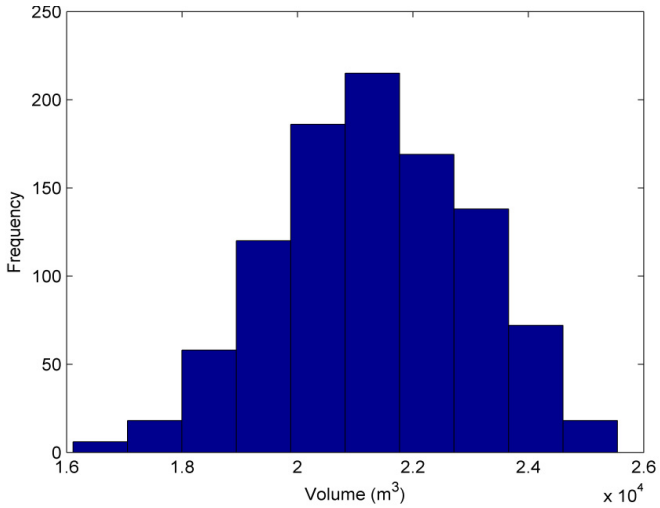

Fig. 10. Distribution of uncertainties in estimating the pore volume of the extracted CO_2 traces.

For the two accumulations analysed here, taken together, the 95% confidence interval for the volume estimation is between about 17000 m^3 and 25000 m^3.

4. Detection thresholds

4.1. Top Utsira Sand

Given that our statistical method can reliably identify individual CO_2 accumulations at the top of the Utsira Sand of around 10000 m^3, it is instructive to determine how small a CO_2 accumulation might be detectable and what accumulations might be mistaken for noise. A set of tests was carried out to test the detectability of synthetic CO_2 accumulations of known size, circular geometry and of uniform reflection amplitude. A range of synthetic accumulations of different radii and different amplitudes was generated and superimposed at random locations on noise-only portions of the area. The process was repeated 1000 times. Wavelet de-noising was applied to each iteration, recording whether or not the synthetic accumulation was correctly detected, and probabilities derived for a range of reflection amplitudes and accumulation areas. The synthetic geometry used in this initial study is very simple; designed to illustrate the principle, and so derived probabilities should be treated as preliminary. Improved synthetic accumulation geometries are under development.

As would be expected, the probability of detecting the accumulation increases with area and reflectivity amplitude (Fig. 11a). Scaling amplitudes to layer thickness (Fig. 11b), it is clear that detection depends on accumulation thickness and area. Very thin layers (< 0.5 m) are difficult to detect irrespective of area (due to their low reflection amplitude) whereas layers > 2 m thick are highly detectable irrespective of area (due to their higher reflection amplitude). For layers between 0.5 and 2 m thick detectability depends on area, so large but thin layers might be detectable.

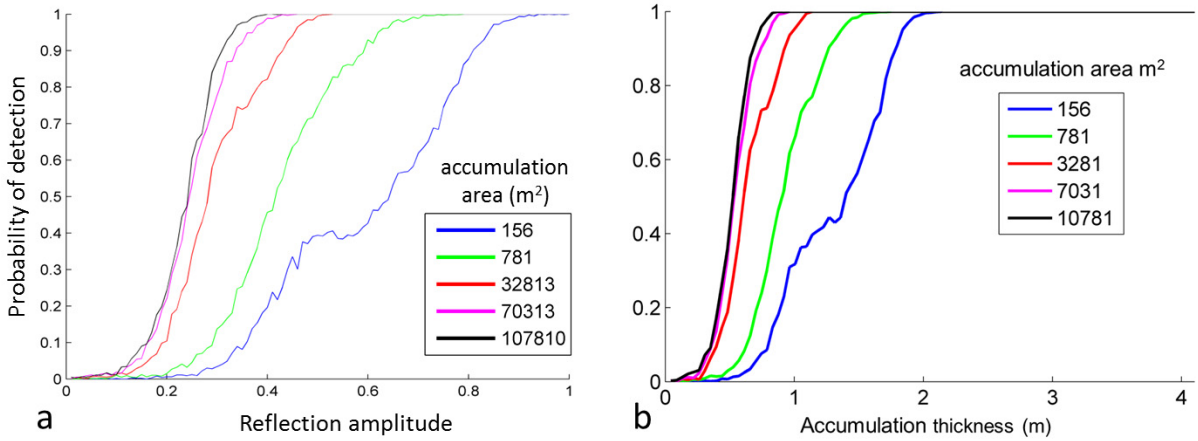

Fig. 11. Probability of detecting circular synthetic CO_2 accumulations as a function of a) reflection amplitude b) thickness

In order to determine detection thresholds in terms of CO_2 amounts, it is necessary to plot the probability of detection against layer pore volume (Fig. 12). As above, detection depends on layer thickness, so very thin layers (large area compared to volume) are difficult to detect. For pore volumes between 500 and 3000 m^3 detectability depends on thickness, so small thick accumulations will be more detectable than larger, thinner ones of the same volume. Accumulations with pore volumes above about 3000 m^3 will be robustly detectable for layer thicknesses > 1m, which will generally be the case.

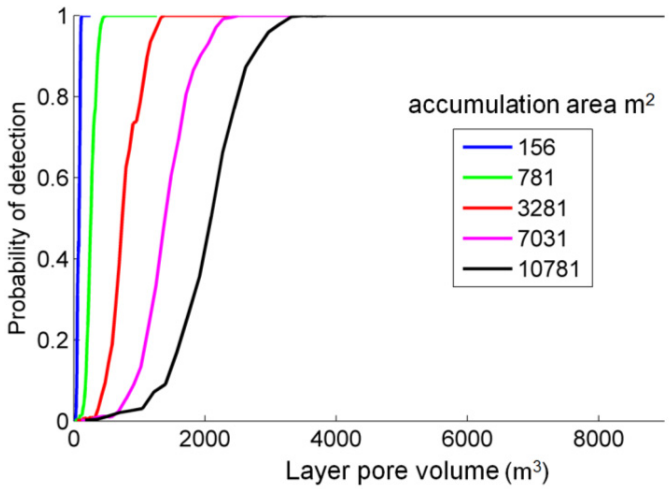

Fig. 12. Probability of detecting circular synthetic CO_2 accumulations against pore volume of feature.

In terms of CO_2 amounts, given an approximate CO_2 density at top Utsira Sand of around 700 kgm^{-3}, and assuming full (100%) CO_2 saturation (the conservative detection end-member), a pore-volume of 3000 m^3 equates to a CO_2 mass of around 2100 tonnes. Lower CO_2 saturations would correspond to a lower detection threshold.

4.2. Overburden

In order to estimate detection limits in the overburden, time-slice amplitude difference maps were generated at two levels (Fig. 13). The first time-slice, at a two-way time of 560 ms (corresponding to a depth of around 490 m), is in a seismically quiet part of the overburden sequence, above the noisy layer with the gas related bright-spots. The second time-slice, at a two-way time of 670 ms (corresponding to a depth of about 590 m), is within the noisier bright-spot sequence, where significant repeatability noise is evident (Fig. 13).

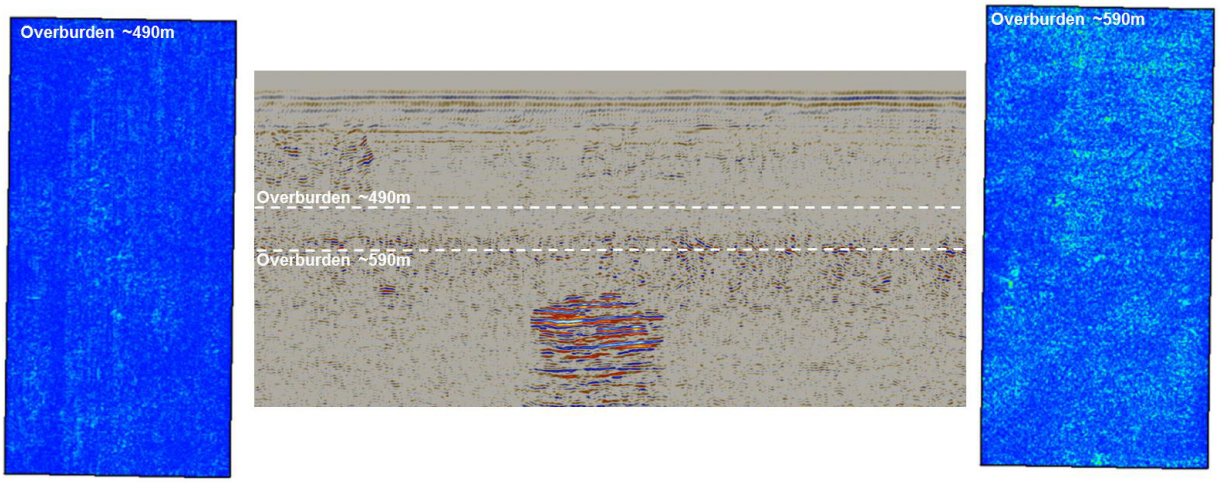

Fig. 13. Amplitude difference time-slices from the overburden. The time-slice at 490 m (left) is markedly quieter than the time-slice from 590 m (right). Two-way time range of the seismic line is 0 - 1300 ms

It is also necessary to take into account the different rock physics at shallower depths. At depths less than around 600 m, CO_2 properties change markedly as it moves into a gaseous phase with marked reductions in bulk modulus (Fig. 14). This increases the reflectivity of a CO_2 accumulation; by a factor of 1.33 at 590 m and a factor of 1.36 at 490m compared to its reflectivity at top Utsira Sand.

It is evident that detection capability will be superior in the shallower, less noisy time-slice. This is borne out by the analysis (Fig. 15). Taking into account the increased reflectivity, accumulations at 490 m depth with pore volumes more than about 2200 m^3 will be robustly detectable for layer thicknesses > 1m. At 590 m depth accumulations with pore volumes more than about 4500 m^3 will be robustly detectable for layer thicknesses greater than 1m.

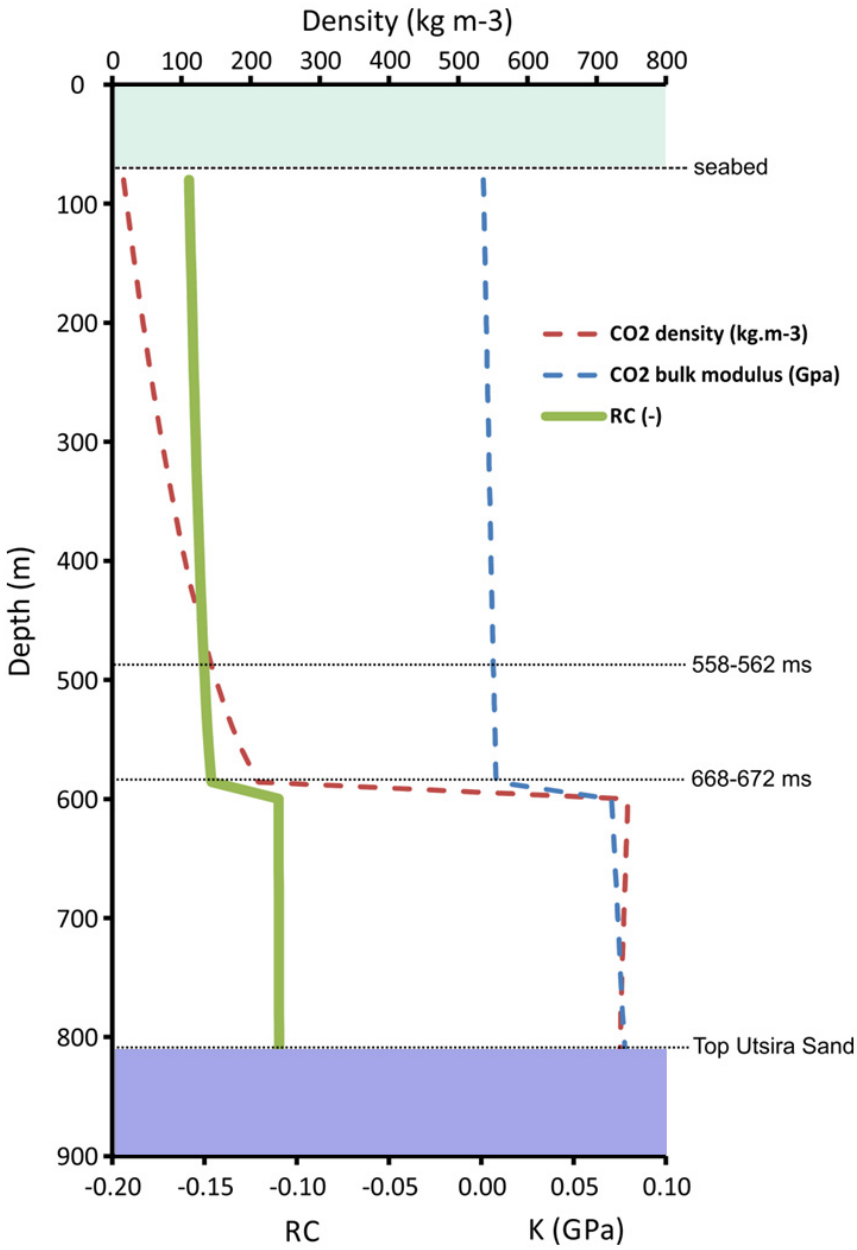

Fig. 14. Changes in CO_2 properties and reflectivity with depth in the Sleipner overburden, dotted lines denote the three analysis levels (Top Utsira Sand, 590 m and 490 m). K = bulk modulus; RC = reflection co-efficient of a sandy layer filled with fully saturated CO_2.

In converting pore volumes to actual CO_2 amounts, an even more significant effect is the reduction in CO_2 density at shallower depths. Thus at 590 m CO_2 density is ~211 kgm^{-3} , reducing further to ~143 kgm^{-3} at 490 m (Fig. 14). Assuming full (100%) CO_2 saturation (the conservative end-member), the above pore-volumes convert to CO_2 masses of 950 tonnes at 590 m and only 315 tonnes at 490 m.

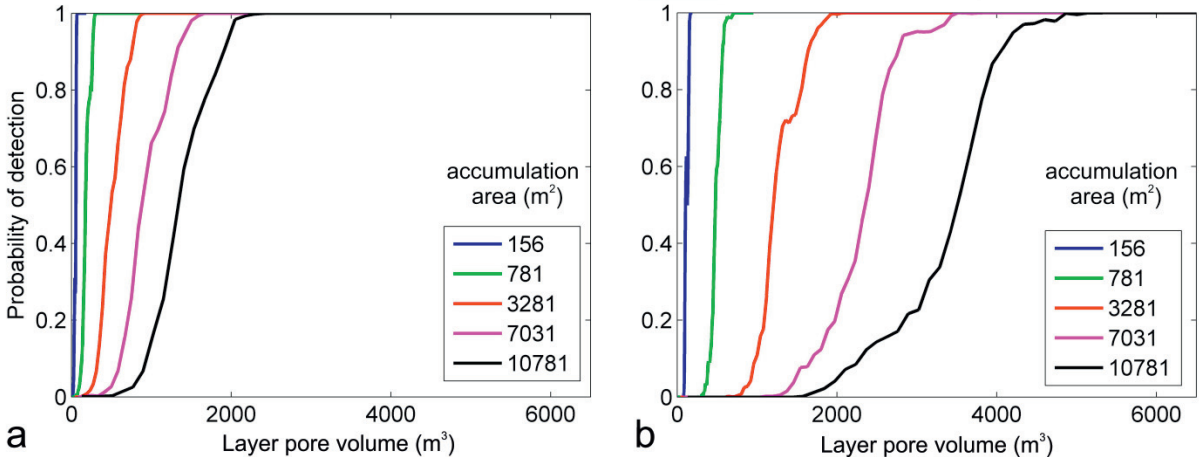

Fig. 15. Probability of detecting synthetic features within the overburden a) at 490 m in quiet data b) at 590 m in noisier difference data

It is clear therefore that detectability varies markedly with depth, and is controlled by levels of repeatability noise and also by CO_2 properties. In general terms detectability improves at shallower depth, governed principally by increasingly reflective gaseous phase CO_2. It is notable however that for conventional 3D offshore data, survey repeatability worsens markedly in the very shallow section beneath the seabed (Fig. 13), as the effects of low folds of cover and strongly inclined ray-paths become important. This will degrade detectability in the shallow section where high resolution 3D surveys such as the p-cable system might be more effective. It should also be emphasised that the tool is still at an early stage of development, with a very simple circular synthetic accumulation model for the probability analysis; this might give rather optimistic detection thresholds compared with real accumulations which are likely to thin towards their edges, giving a less spatially sharp seismic signal. Work is ongoing to refine the synthetic accumulation model to make it more realistic.

5. Conclusions

A methodology has been developed to determine the detectability of small accumulations of CO_2 using time-lapse 3D seismics. It operates on time-slices through difference cubes and depends on the CO_2 accumulation producing a reflectivity change due to fluid substitution effects. The method is statistically based and shows that detectability is a function of both reflection amplitude and lateral extent. The tool is currently at an early stage of development, with a very simple circular synthetic accumulation model for the probability analysis, but as ongoing improvements are incorporated it should be feasible to determine pore volumes that will likely prove to be robustly detectable.

It is not possible to determine a single detection limit for a given dataset, as detectability varies markedly with depth, and the selection of an optimal overburden monitoring horizon might well be decided on this basis.

Detection capability can be equated to the maximum allowable leakage rate consistent with a storage site meeting its greenhouse gas emissions mitigation objective. A number of studies have suggested that leakage rates around 0.01% per year or less would ensure effective mitigation performance [11]. So for a hypothetical large-scale storage project, injecting around 100 Mt of CO_2, the detection capability of the Sleipner seismics would be some two orders of magnitude below the effective mitigation leakage limit. It is likely therefore that well designed 3D seismic monitoring systems will have detection capability significantly superior to what is required to prove greenhouse gas mitigation efficacy.

6. Acknowledgements

This paper is published with permission of the Executive Director British Geological Survey (NERC). The work was carried out within the CO2CARE project which is funded by the European Commission within the 7th Framework Programme and also co-financed by an industrial consortium consisting of RWE, Shell, Statoil, TOTAL, Vattenfall and Veolia. The financial support of the EC and the industry partners is greatly appreciated.

References

[1] Implementation of Directive 2009/31/EC on the Geological Storage of Carbon Dioxide. Guidance Document 2: Characterisation of the Storage Complex, CO2 Stream Composition, Monitoring and Corrective Measures. ISBN-13 978-92-79-19834-2, DOI: 10.2834/98293. 2011.

[2] Baklid A, Korbøl R, Owren, G. Sleipner Vest CO_2 disposal, CO_2 injection into a shallow underground aquifer. SPE paper 36600, presented at 1996 SPE Annual Technical Conference and Exhibition, Denver Colorado, USA, 6-9 October 1996.

[3] Korbøl R, Kaddour A. Sleipner Vest CO_2 disposal – injection of removed CO2 into the Utsira Formation. In: Kondo, J., Inui, T., Wasa, K. (Eds). Proceedings of the second International Conference on Carbon Dioxide Removal, Kyoto 24-27 October 1994. Pergamon, 519-512.

[4] Arts RJ, Chadwick RA, Eiken O, Thibeau S, Nooner S. 2008, Ten years' experience of monitoring CO_2 injection in the Utsira Sand at Sleipner, offshore Norway: First Break 2008; 26:65-72.

[5] Chadwick RA, Arts R, Eiken, O. 4D seismic quantification of a CO_2 plume at Sleipner, North Sea. In: Dore AG, Vining B, editors. Petroleum Geology: North West Europe and Global Perspectives: Proceedings of the 7th Petroleum Geology Conference, Published by the Geological Society, London, 2005; 1385–1399.

[6] White DJ. 2014. Toward quantitative CO_2 storage estimates from time-lapse 3D seismic travel-times: An example from the IEAGGH Weyburn-Midale monitoring and storage project. International Journal of Greenhouse Gas Control 2014; 16S: S95-S102.

[7] Chadwick RA, Arts R, Eiken O, Kirby GA, Lindeberg E, Zweigel P. 2004, 4D seismic imaging of a CO_2 plume at the Sleipner Field, central North Sea. In: Davies RJ, Cartwright JA, Stewart SA, Lappin M, Underhill JR, editors. 3-D Seismic Technology: Application to the Exploration of Sedimentary Basins, Geological Society, London; 2004. p. 311-320.

[8] Coifman RR, Donoho DL, Antoniadis A, Oppenheim G. Translation-invariant de-noising, Wavelets and Statistics. Springer-Verlag. 1995.

[9] Buades A, Coll B, Morel JM. A Review of Image Denoising Algorithms with a New One, Multiscale Modeling & Simulation, 2005; 4/2: 490-530.

[10] Kumar P, Foufoula-Georgiou E. Wavelet Analysis in Geophysics: An Introduction. In: Foufoula-Georgiou E, Kumar P, editors. Wavelets in Geophysics. Academic Press; 1994, 1-45.

[11] Hepple RP, Benson SM. Implications of surface seepage on the effectiveness of geological storage of carbon dioxide as a climate change mitigation option. In: Gale J, Kaya Y, editors. Greenhouse Gas Control Technologies. Volume 1, Elsevier Science Ltd, Oxford, UK; 2003. p. 261–266.